Available online at www.sciencedirect.com
SCIENCE DIRECT®
Comput. Methods Appl. Mech. Engrg. 193 (2004) 2087–2104
Computer methods in applied mechanics and engineering
www.elsevier.com/locate/cma

A monolithic approach to fluid–structure interaction using space–time finite elements

Björn Hübner, Elmar Walhorn, Dieter Dinkler *

Institut für Statik, Technische Universität Braunschweig, Beethovenstr. 51, 38106 Braunschweig, Germany

Received 3 December 2002; received in revised form 20 November 2003; accepted 2 January 2004

Abstract

The paper presents a simultaneous solution procedure for fluid–structure interaction problems. The structural motion is described by geometrically nonlinear elastodynamics. The fluid is modeled by the incompressible Navier–Stokes equations. The space–time finite element method is applied to both continua leading to an almost uniform discretization in which velocity variables are used for fluid and structure. In order to enforce momentum conservation and geometric continuity at the interface, a weighted residual formulation of coupling conditions is introduced. The discretized model equations for fluid, structure and coupling conditions are formulated in a single equation system. The nonlinear system and the fluid mesh movement are solved in a single iteration loop. Two-dimensional examples of membrane flutter and vortex excited plate vibrations demonstrate the efficiency of the methodology.

Keywords: Fluid–structure interaction; Simultaneous solution; Space–time finite elements; Nonlinear elastodynamics; Incompressible Navier–Stokes equations

1. Introduction

In order to reduce development time and cost in aerospace, automotive and mechanical engineering or to construct exceptional civil engineering structures, the numerical simulation of coupled systems becomes more and more important. In case of long-span bridges, high-rise buildings and lightweight roof structures, the interaction of wind flow and structural motion may lead to aeroelastic instabilities, see [1], which may cause the collapse of the structure. Fluid–structure interaction has to be considered for fluid conveying flexible tubes and pipes or liquid-filled tanks due to dynamic excitation, too. Moreover, in life sciences, a better insight into the phenomenology of blood flow through healthy and diseased arteries may support the therapy of atherosclerosis, see [2,3]. Realistic models of such problems have to describe large structural deformations interacting with viscous fluids.

The development of efficient and accurate solvers for complex fluid–structure interaction problems is still a challenging task in research. In case of time-dependent nonlinear fluid models like the Euler or

* Corresponding author. Tel.: +49-531-391-3667; fax: +49-531-391-8116.
E-mail address: statik@tu-bs.de (D. Dinkler).

0045-7825/$ - see front matter
doi:10.1016/j.cma.2004.01.024

Navier–Stokes equations, which are coupled with linear or nonlinear elastic structures, the solution strategies range from partitioned solutions with loose coupling algorithms over partitioned solutions with strong coupling up to simultaneous solutions. In loose coupling algorithms, separate solvers for fluid and structure are applied once per time step, leading to a time lag between both continua. The method, which is widely used due to the simplified coupling procedure (e.g. [4–8]) is appropriate for weak interactions between fluid and structure and may diverge in case of strong interactions. An additional iteration loop over the partial solvers leads to strongly coupled partitioned solutions (e.g. [9–12]), which show better convergence and stability characteristics at the expense of additional numerical effort. In both methods, subcycling is possible, for example, if the time scales in the flow field are much smaller than structural time scales. Another advantage of the partitioned solution approach is the application of existing appropriate and sophisticated solvers for each subsystem, which may be replaced with little effort.

In case of strong interactions, simultaneous solution procedures may be preferable in order to ensure stability and to accelerate convergence of the coupled solution. In the broader sense, simultaneous procedures solve the coupled system in a single iteration loop with consistent time integration schemes for all physical fields, see [13,14], or [15], leading to time accurate coupled solutions. In the narrower sense, a single equation system for the entire problem has to be formulated and solved simultaneously, see [16,12,17,18], or [19]. If the discretization methods are equal in all subsystems, a monolithic method follows, in which the coupled system is regarded as a whole. This enables mathematical analyses of coupled systems and ensures convergence, even if the subsystem behavior strongly differs from the fully coupled system, provided that the nonlinearities of the subsystems can be resolved. However, in simultaneous solution procedures the time step has generally to be equal in all subsystems, which may be inefficient, if different time scales are present. Furthermore, the formulation of a single equation system may lead to ill-conditioned system matrices including zero entries on the diagonal. Thus, appropriate preconditioners for the iterative solution of these large sparse linearized systems on parallel computing platforms are difficult to find. In addition, the development, implementation and validation of a completely new solver is required.

The present article deals with the simultaneous solution of nonlinear elastic structures interacting with incompressible viscous fluids. In the monolithic approach, the discrete forms of fluid mass conservation and momentum conservation for the entire fluid–structure system are formulated in a single equation system and solved with the fluid mesh movement in a single iteration loop. Time-discontinuous stabilized space–time finite elements are applied to discretize all model equations, leading to a nearly uniform discretization of the entire system.

The space–time finite element method provides a consistent discretization of both space and time domain including space–time adaptive meshes, which enable the temporal discretization to vary over the spatial domain. Furthermore, the method implies a natural description of moving fluid domains, since isoparametric space–time elements are adaptable in time direction. In elastodynamics, time-discontinuous stabilized space–time elements were introduced by Hughes and Hulbert [20], who applied the formulation to wave propagation problems. For fluid dynamics Brooks and Hughes [21] and Hughes et al. [22] presented stabilized finite elements, while Tezduyar et al. [23] and Hansbo [24] applied the space–time formulation for solving the incompressible Navier–Stokes equations on moving meshes. In this context, solution strategies for large-scale flow simulations were presented by Behr and Tezduyar [25] and mesh update strategies in parallel computations by Johnson and Tezduyar [26].

2. Model equations

In order to describe large structural displacements and rotations, a geometrically nonlinear theory is applied. The model equations are given in a total Lagrangian representation using a mixed formulation with velocities and 2nd Piola–Kirchhoff stresses as primal variables. The flow field is modeled by the

Navier–Stokes equations for incompressible fluids using a velocity-pressure formulation. The governing equations of the fluid are defined in a time-dependent domain, which has moving boundaries as a result of structural deformations. If high Reynolds number flows appear, e.g. in case of building aeroelasticity, turbulence effects are essential for flow characteristics and have to be considered. For this purpose, Reynolds averaging of the Navier–Stokes equations in conjunction with the k–ω turbulence model by Wilcox [27] will extend the fluid formulation in the future. In addition, coupling conditions for velocity and traction are defined on the fluid–structure interface.

2.1. Elastodynamics

The time-dependent deformation of elastic structures is described by the nonlinear partial differential equations

$$\rho_0 \dot{\mathbf{v}} - \operatorname{div}_0(\mathbf{FS}) - \mathbf{f}_0 = \mathbf{0} \quad \text{in } Q_0, \tag{1}$$

$$\underline{\mathbf{C}}^{-1} \cdot\cdot \dot{\mathbf{S}} - \dot{\mathbf{E}}(\mathbf{v}, \mathbf{u}) = \mathbf{0} \quad \text{in } Q_0, \tag{2}$$

which fulfill momentum conservation and the constitutive law for a St. Venant–Kirchhoff material. The constitutive law is given in rate formulation, leading to a mixed formulation with two partial differential equations of first order in time. The model equations are defined in the reference space–time domain $Q_0 = \Omega_0 \times (0, T)$ with the boundary $P_0 = \Gamma_0 \times (0, T)$. The index 0 denotes the reference configuration, corresponding to the differential operators div_0 and grad_0. In Eqs. (1) and (2) ρ denotes the density, $\mathbf{v} = \dot{\mathbf{u}}$ the velocity vector and $\mathbf{u}$ the displacement vector. $\mathbf{S}$ is the 2nd Piola–Kirchhoff stress tensor and $\mathbf{F} = \mathbf{I} + \operatorname{grad}_0 \mathbf{u}$ the deformation gradient, where $\mathbf{I}$ is the identity tensor. $\mathbf{f}$ denotes the body force vector. The fourth order tensor of elasticity $\underline{\mathbf{C}}$ is assumed to be time invariant. However, even more complex constitutive equations can be used within the mixed velocity–stress formulation, which is particularly suitable for viscoelastic and viscoplastic material laws, e.g. [28]. The substantial derivative of the Green–Lagrangian strain tensor $\mathbf{E}$ leads to the nonlinear kinematic relation

$$\dot{\mathbf{E}}(\mathbf{v}, \mathbf{u}) = \tfrac{1}{2}\Big(\operatorname{grad}_0 \mathbf{v} + (\operatorname{grad}_0 \mathbf{v})^{\mathrm{T}}\Big) + \tfrac{1}{2}\Big((\operatorname{grad}_0 \mathbf{u})^{\mathrm{T}} \operatorname{grad}_0 \mathbf{v} + (\operatorname{grad}_0 \mathbf{v})^{\mathrm{T}} \operatorname{grad}_0 \mathbf{u}\Big). \tag{3}$$

The boundary $P_0 = P_0^g \cup P_0^h$ is subdivided into a Dirichlet part P_0^g and a Neumann part P_0^h with the boundary conditions

$$\mathbf{v} = \mathbf{g} \ \text{ on } P_0^g \quad \text{and} \quad \mathbf{t}_0 = \mathbf{h}_0 \ \text{ on } P_0^h, \tag{4}$$

where $\mathbf{g}$ and $\mathbf{h}_0$ are prescribed values of velocities and tractions, respectively. The vector of boundary tractions $\mathbf{t}_0 = (\mathbf{FS}) \cdot \mathbf{n}_0$ is defined using the unit outward normal vector $\mathbf{n}_0$ of the spatial boundary. The initial conditions

$$\mathbf{u}(t = 0) = \mathbf{u}_i, \quad \mathbf{v}(t = 0) = \mathbf{v}_i \ \text{ in } \Omega_0 \tag{5}$$

specify given values of displacements $\mathbf{u}_i$ and velocities $\mathbf{v}_i$ in the spatial domain Ω_0 at the time $t = 0$.

2.2. Fluid dynamics

The incompressible Navier–Stokes equations, consisting of momentum conservation and continuity equation

$$\rho\left(\frac{\partial \mathbf{v}}{\partial t} + \mathbf{v} \cdot \operatorname{grad} \mathbf{v}\right) - \operatorname{div} \mathbf{T} - \mathbf{f} = \mathbf{0} \quad \text{in } Q, \tag{6}$$

$$\operatorname{div} \mathbf{v} = 0 \quad \text{in } Q, \tag{7}$$

are defined in the moving space–time domain $Q = \Omega_t \times (0,T)$ with the boundary $P = \Gamma_t \times (0,T)$. The Cauchy stress tensor

$$\mathbf{T} = 2\mu \mathbf{D}(\mathbf{v}) - p\mathbf{I} \tag{8}$$

depends for Newtonian fluids linearly on the strain rate tensor

$$\mathbf{D}(\mathbf{v}) = \tfrac{1}{2}\Big(\operatorname{grad} \mathbf{v} + (\operatorname{grad} \mathbf{v})^{\mathrm{T}}\Big) \tag{9}$$

and the pressure p, which is used as primal variable in addition to the velocity. The linear material behavior is characterized by the dynamic viscosity μ. The Dirichlet and Neumann boundary conditions of the flow field

$$\mathbf{v} = \mathbf{g} \text{ on } P^g \quad \text{and} \quad \mathbf{t} = \mathbf{h} \text{ on } P^h \tag{10}$$

with the boundary tractions $\mathbf{t} = \mathbf{T} \cdot \mathbf{n}$ of the instantaneous configuration specify the given values of velocities and tractions on complementary boundary subsets. The initial condition

$$\mathbf{v}(t=0) = \mathbf{v}_i \quad \text{with } \operatorname{div} \mathbf{v}_i = 0 \text{ in } \Omega_0 \tag{11}$$

specifies a divergence free velocity field at the time $t = 0$.

2.3. Coupling conditions

In order to get a complete model of the coupled system, composed of instationary flow field and elastic body, coupling conditions are required on the interface $P^{\mathrm{c}} = P^{\mathrm{F}} \cap P^{\mathrm{S}}$. The indices F and S denote the fluid and the structural part, respectively. The geometric continuity is enforced by the condition

$$\mathbf{v}^{\mathrm{F}} - \mathbf{v}^{\mathrm{S}} = \mathbf{0} \quad \text{on } P^{\mathrm{c}}, \tag{12}$$

which implies that the fluid boundary has to follow the structural displacements. Momentum conservation on the interface is enforced by the condition

$$\mathbf{t}_0^{\mathrm{S}} + \frac{\mathrm{d}\Gamma_t}{\mathrm{d}\Gamma_0}\mathbf{t}^{\mathrm{F}} = \mathbf{0} \quad \text{on } P_0^{\mathrm{c}}, \tag{13}$$

which demands equal tractions. Therefore, the fluid tractions are projected onto the reference configuration with opposite sign, since the unit outward normal vectors of fluid and structure have opposite directions.

3. Space–time discretization

A single discretization method is applied to the coupled system, using stabilized space–time finite elements for fluid and structural dynamics. Space–time finite elements are parametrized in space and time directions, leading to a consistent discretization of both space and time domain. The space–time domain Q is subdivided into a sequence of space–time slabs $Q_n = \Omega_t \times (t_n, t_{n+1})$, see Fig. 1 (left), since the future cannot influence the past. Thus, an efficient numerical scheme follows. The application of isoparametric space–time elements leads directly to a discretization of model equations in moving domains, corresponding to the Arbitrary Lagrangian–Eulerian (ALE) formulation, see [23–25]. Moreover, the space–time formulation satisfies inherently the geometric conservation law (GCL), see [29], if continuous shape functions for the geometry and a sufficiently accurate quadrature for integration are used.

The interpolation of physical variables is discontinuous in time, see Fig. 1 (right), with independent degrees of freedom in adjoining time slabs at discrete time levels t_n. The time-discontinuous Galerkin

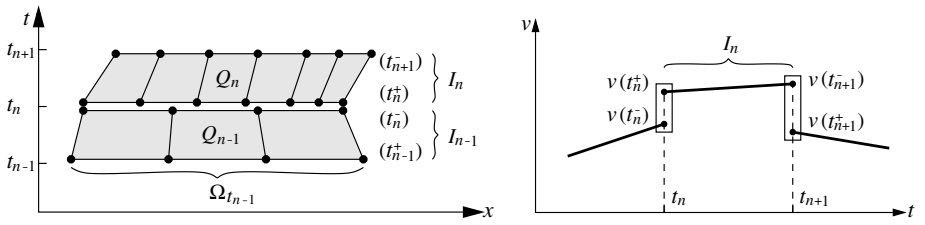

Fig. 1. Moving space–time mesh and time-discontinuous interpolation.

formulation results in an implicit time integration scheme, which is A-stable and accurate of third order, when linear interpolation functions are used, see [30,31]. The continuity of primal variables is achieved in integral form using jump terms in the variational formulation. This includes projections of the solution, if remeshing is necessary, see [24].

A Petrov–Galerkin stabilization of space–time elements prevents numerical oscillations in solutions to hyperbolic differential equations, see [21,22], comparable with second order upwind schemes. The stabilization term extends the standard Galerkin weighting function and introduces additional numerical diffusion. The method provides stable solutions to the Navier–Stokes equations for a wide range of Reynolds numbers and allows the application of interpolation functions of equal order for velocities and pressure, see [23].

3.1. Elastodynamics

The stabilized space–time finite element formulation of the structural part within the time slab $Q_{0,n}$ including boundaries $P_{0,n}$ reads

$$\int_{Q_{0,n}} \delta\mathbf{v}\cdot\rho_0\dot{\mathbf{v}}\,\mathrm{d}Q_0 + \int_{Q_{0,n}} \dot{\mathbf{E}}(\delta\mathbf{v},\mathbf{u})\cdot\mathbf{S}\,\mathrm{d}Q_0 - \int_{Q_{0,n}} \delta\mathbf{v}\cdot\mathbf{f}_0\,\mathrm{d}Q_0 \tag{14a}$$

$$+\sum_e \int_{Q^e_{0,n}} \delta\mathbf{S}\cdot\cdot\left(\underline{\mathbf{C}}^{-1}\cdot\cdot\mathbf{S} - \dot{\mathbf{E}}(\mathbf{v},\mathbf{u})\right)\mathrm{d}Q_0 \tag{14b}$$

$$+\int_{\Omega_0} \delta\mathbf{v}(t_n^+)\cdot\rho_0\big(\mathbf{v}(t_n^+)-\mathbf{v}(t_n^-)\big)\mathrm{d}\Omega_0 \tag{14c}$$

$$+\sum_e \int_{\Omega^e_0} \delta\mathbf{S}(t_n^+)\cdot\cdot\,\underline{\mathbf{C}}^{-1}\cdot\cdot\big(\mathbf{S}(t_n^+)-\mathbf{S}(t_n^-)\big)\mathrm{d}\Omega_0 \tag{14d}$$

$$+\sum_e \int_{Q^e_{0,n}} \tau_{\mathrm{M}}^{\mathrm{S}}\delta\dot{\mathbf{v}}\cdot\left(\rho_0\dot{\mathbf{v}} - \mathrm{div}_0(\mathbf{F}\mathbf{S}) - \mathbf{f}_0\right)\mathrm{d}Q_0 \tag{14e}$$

$$-\int_{P^g_{0,n}} \delta\mathbf{v}\cdot\mathbf{t}_0\,\mathrm{d}P_0 + \int_{P^g_{0,n}} \delta\mathbf{t}_0\cdot(\mathbf{v}-\mathbf{g})\,\mathrm{d}P_0 \tag{14f}$$

$$-\int_{P^h_{0,n}} \delta\mathbf{v}\cdot\mathbf{h}_0\,\mathrm{d}P_0 = 0 \quad \forall\,\delta\mathbf{v},\delta\mathbf{S},\delta\mathbf{t}_0, \tag{14g}$$

where e runs over all elements. All time slabs are solved successively, and the initial conditions are given by

$$\mathbf{v}(t_0^-) = \mathbf{v}_i,$$

$$\mathbf{S}(t_0^-) = \underline{\mathbf{C}}\cdot\cdot\tfrac{1}{2}\Big(\mathrm{grad}_0\mathbf{u}_i + (\mathrm{grad}_0\mathbf{u}_i)^{\mathrm{T}} + (\mathrm{grad}_0\mathbf{u}_i)^{\mathrm{T}}\mathrm{grad}_0\mathbf{u}_i\Big). \tag{15}$$

Time integration of velocities results in the displacement field $\mathbf{u}(\mathbf{x},t)$, which is used for computing the strain rate tensor $\dot{\mathbf{E}}$ and for localizing the current fluid–structure interface. In Eq. (14), line (a) represents the weak form of momentum conservation and line (b) fulfills the constitutive law at the element level. The jump terms for velocities (c) and stresses (d) satisfy the initial conditions of the time slab in integral form. The stabilization term, which is applied in case of wave propagation problems, is shown in line (e). For the parameter $\tau_{\mathrm{M}}^{\mathrm{S}}$, the definition by Hughes and Hulbert [20] is used. The last two lines (f) and (g) represent the integral form of the Dirichlet boundary condition and the surface load term of the Neumann condition, respectively.

In the two-dimensional numerical model, 8-noded space–time hexahedron-elements are employed, using a piecewise bilinear interpolation in space and a discontinuously linear interpolation in time for the velocity components. The interpolation of tractions is piecewise linear in space and discontinuously linear in time. On the other hand, the interpolation of stress components is discontinuous in space and time. Due to the mixed-hybrid formulation, similar to Pian and Tong [32], the interpolation functions are defined only inside the elements. Using an appropriate least-order interpolation with five degrees of freedom in space for the local stress components, which refer to the covariant basis of local element coordinates, a stable invariant element formulation follows, see [33]. After static condensation of stress variables on element level, velocities and boundary tractions are global degrees of freedom. Even for extremely stretched elements, the formulation provides stable solutions without shear locking. However, the formulation is not valid for fully incompressible materials. In this case, the structural part has to be modeled by a three-field formulation using velocity, pressure and deviatoric stress variables, see [34]. The presented coupling and simultaneous solution procedure will remain unaffected by this modification.

3.2. Fluid dynamics

The stabilized space–time finite element formulation of the fluid model reads

$$\int_{Q_n} \delta\mathbf{v}\cdot\rho\left(\frac{\partial\mathbf{v}}{\partial t}+\mathbf{v}\cdot\operatorname{grad}\mathbf{v}\right)\mathrm{d}Q+\int_{Q_n}\mathbf{D}(\delta\mathbf{v})\cdot\cdot\,2\mu\mathbf{D}(\mathbf{v})\,\mathrm{d}Q \tag{16a}$$

$$-\int_{Q_n}(\operatorname{div}\delta\mathbf{v})p\,\mathrm{d}Q-\int_{Q_n}\delta\mathbf{v}\cdot\mathbf{f}\,\mathrm{d}Q \tag{16b}$$

$$+\int_{Q_n}\delta p\operatorname{div}\mathbf{v}\,\mathrm{d}Q \tag{16c}$$

$$+\int_{\Omega_n}\delta\mathbf{v}(t_n^+)\cdot\rho\big(\mathbf{v}(t_n^+)-\mathbf{v}(t_n^-)\big)\mathrm{d}\Omega \tag{16d}$$

$$+\sum_e\int_{Q_n^e}\tau_{\mathrm{M}}^{\mathrm{F}}\frac{1}{\rho}\mathscr{L}(\delta\mathbf{v},\delta p)\cdot(\mathscr{L}(\mathbf{v},p)-\mathbf{f})\mathrm{d}Q \tag{16e}$$

$$+\sum_e\int_{Q_n^e}\tau_C^{\mathrm{F}}\rho(\operatorname{div}\delta\mathbf{v})\operatorname{div}\mathbf{v}\,\mathrm{d}Q \tag{16f}$$

$$-\int_{P_n^g}\delta\mathbf{v}\cdot\mathbf{t}\,\mathrm{d}P+\int_{P_n^g}\delta\mathbf{t}\cdot(\mathbf{v}-\mathbf{g})\,\mathrm{d}P \tag{16g}$$

$$-\int_{P_n^h}\delta\mathbf{v}\cdot\mathbf{h}\,\mathrm{d}P=0\quad\forall\,\delta\mathbf{v},\ \delta p,\ \delta\mathbf{t}, \tag{16h}$$

where the differential operator

$$\mathscr{L}(\mathbf{v},p)=\rho\left(\frac{\partial\mathbf{v}}{\partial t}+\mathbf{v}\cdot\operatorname{grad}\mathbf{v}\right)-\operatorname{div}(2\mu\mathbf{D}(\mathbf{v})-p\mathbf{I}) \tag{17}$$

describes the strong form of momentum conservation (6) without the body force term. Apart from the weighted residual formulation of the Dirichlet boundary condition in line (g), Eq. (16) is identical to the formulation of Behr and Tezduyar [25], including the definition of the stabilization parameters $\tau_{\mathrm{M}}^{\mathrm{F}}$ in line (e) and τ_{C}^{F} in line (f). The interpolation functions for velocity and pressure variables are piecewise bilinear in space and discontinuously linear in time, while the geometry interpolation is piecewise bilinear in space and piecewise linear or quadratic in time.

3.3. Fluid–structure coupling

The space–time finite element formulation of the coupling conditions (12) and (13) uses traction variables $\mathbf{t}$ on the interface in order to fulfill geometric continuity and momentum conservation between fluid and structure in weighted residual form. In particular, the preset velocity values of the Dirichlet boundary conditions of the fluid (16 g) are substituted by structural velocities

$$-\int_{P_n^{\mathrm{c}}}\delta\mathbf{v}^{\mathrm{F}}\cdot\mathbf{t}^{\mathrm{F}}\,\mathrm{d}P+\int_{P_n^{\mathrm{c}}}\delta\mathbf{t}^{\mathrm{F}}\cdot(\mathbf{v}^{\mathrm{F}}-\mathbf{v}^{\mathrm{S}})\,\mathrm{d}P \tag{18}$$

and the fluid boundary tractions act as surface loads onto the structure

$$-\int_{P_{0,n}^{\mathrm{c}}}\delta\mathbf{v}^{\mathrm{S}}\cdot\left(-\frac{\mathrm{d}\Gamma_t}{\mathrm{d}\Gamma_0}\mathbf{t}^{\mathrm{F}}\right)\mathrm{d}P_0. \tag{19}$$

In case of matching grids, the coupling condition for velocities is fulfilled numerically exact, and the transfer of information is identical in both directions. For nonmatching grids, a mortar element method follows, which offers mathematical optimality with respect to the global discretization error of the coupled system, see [35], if the integration is performed exactly.

3.4. Mesh moving scheme

The total Lagrangian formulation of the structure is defined in the reference domain, whereas the fluid formulation is based on the instantaneous configuration. Consequently, structural deformations cause moving boundaries of the flow field, and the fluid domain has to be adapted to the current position of the interface. Since iso- or superparametric space–time elements allow the specification of arbitrary displacements of mesh nodes, the mesh boundary of the fluid can move with the structure. However, inside the fluid domain, new positions of the mesh points have to be defined in order to avoid overlapping elements. Therefore, the fluid domain is supposed to be an artificial elastic continuum on which the real structural displacements are imposed, similarly to mesh moving schemes proposed by Lynch [36], Johnson and Tezduyar [26] and others. In order to reduce distortions of extremely stretched elements in boundary layers forming along the interface, an element-wise constant stiffness distribution is applied, which is correlated with the inverse of the smallest edge length of each element. For relatively small two-dimensional examples as presented here, the equations are solved by a direct Cholesky solver. The decomposed system matrix is stored and used in every mesh moving step. In this case, the required CPU-time is negligible.

4. Solution strategy

The discretized model equations of the coupled system are composed of structural (14) and fluid formulation equation (16) as well as coupling conditions (18) and (19). In addition, the fluid domain depends on structural displacements. The resulting nonlinear system of equations has to be solved iteratively. For this purpose, the complete set of nonlinear equations for the current time slab, including fluid mesh dynamics, is solved in a single iteration loop, see Fig. 2 (left). In structural dynamics the Newton–Raphson method is usually preferred as iteration scheme, resulting in quadratic convergence, if an exact Jacobian matrix is used. However, for convection dominated fluid flow, the method has little relevance, see for example [37], since it may diverge in case of large time steps. Moreover, the determination of the exact Jacobian matrix is very costly or impossible, e.g. for moving fluid domains. Therefore, a Picard iteration is used for the linearization of all equations, leading to a relatively simple fixed point type solution procedure, without evaluating the Jacobian matrix. The ith iteration step for the calculation of the unknowns $\hat{\mathbf{x}}_n$ of the nth time slab can be written as

$$\hat{\mathbf{A}}(\hat{\mathbf{x}}_n^{i-1}) \cdot \hat{\mathbf{x}}_n^i = \hat{\mathbf{b}}(\hat{\mathbf{x}}_{n-1}^i, \hat{\mathbf{x}}_n^{i-1}). \tag{20}$$

Here, the unknown values of structural displacements in Eq. (3), convective velocities in Eq. (6), and fluid mesh coordinates in Eq. (15) are treated as known, applying the values of the previous iteration step. In the first step, the solution at the end of the previous time slab is used as a first estimate for the velocity field in the current time slab. For structural displacements and fluid mesh coordinates, a linear extrapolation follows.

The linearized model equations of fluid, structure, and coupling conditions, which enforce mass and momentum conservation of the coupled system, are solved simultaneously in a single equation system, as shown in Fig. 2 (right) without fluid pressure variables. The pseudo-structure of the mesh moving scheme is solved subsequently, since the coordinates of the fluid mesh are treated as known in the linearized model equations. When the iteration has converged, the equation system in Fig. 2 (right) describes the behavior of the fully coupled system in the current space–time slab. Mathematical analyses of the equation system may give information about the stability of the solution procedure. In the examples presented in the following section, the nonlinear coupled solution is reached in all time slabs within only two to four iteration steps. The good convergence properties are achieved for applications with strong interactions and large structural deformations, even without using a Newton–Raphson iteration scheme for the structural part.

In order to solve the large sparse systems of linearized equations, a preconditioned BiCGStab solver is applied. For unstructured grids, renumbering of the unknowns is performed using a reverse Cuthill–McKee

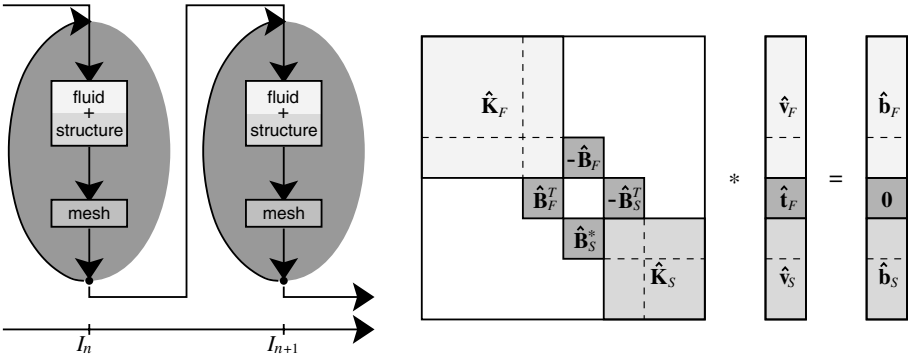

Fig. 2. Simultaneous solution procedure and coupled equation system.

algorithm, which improves allocation and condition of the matrix. A major difficulty is the choice of an appropriate preconditioner for the linear system of equations, since the matrix contains zero entries on the diagonal and may be ill-conditioned for coupled systems. Consequently, common preconditioning procedures as SOR or simple ILU methods do not work or do not accelerate the convergence of the solver. Therefore, a direct LU-decomposition of the matrix is chosen, which is used for preconditioning in the following 10–30 time slabs corresponding to 30–100 nonlinear iteration steps. Here, the BiCGStab solver only needs 1–25 iterations, leading to an efficient solution technique for smaller examples. However, even if the decomposed matrix is stored with a skyline profile technique, the procedure is not applicable to large three-dimensional examples, because an efficient parallel version for high-performance computing is hardly possible.

5. Numerical examples

By means of numerical examples, accuracy, efficiency, and versatility of the presented methodology are discussed. In the first example, a coupled piston-channel system with an extremely varying fluid domain is investigated. The second example deals with two-dimensional laminar flow around a building, interacting with nonlinear vibrations of the membrane roof. Finally, a thin elastic beam structure is analyzed in the wake of a square cylinder.

5.1. Piston

In order to check the implementation of the simultaneous solution procedure and to investigate the accuracy of time integration, a simple piston-channel system is regarded. The configuration with all dimensions is given in Fig. 3. At the left side of the channel, which is filled with an incompressible fluid, an elastic piston is situated. The prescribed velocity $g(t)$, which is imposed at the left side of the piston, increases with constant acceleration of 0.2 m/s^2 from 0 to 2 m/s within 10 s. At the end of this process, the area of the fluid domain is nearly zero. At the outflow boundary, zero pressure conditions are valid, while slip boundary conditions are used at the channel walls. Consequently, the fluid viscosity has no influence, and the system behavior becomes one-dimensional.

The fluid density is $\rho_F = 1$ kg/m^3. The density of the piston is assumed to be nearly zero, while Young's modulus and Poisson's ratio are given by $E = 10$ N/m^2 and $v = 0$, respectively. The system can be considered as a single mass oscillator with strongly nonlinear properties due to the dramatically changing mass. The elastic piston acts as a linear spring and the fluid as a variable mass. For coupled systems of this type, partitioned solutions usually diverge, even for iterative coupling procedures with strong under-relaxation.

The piston is discretized with a space–time hexahedron-element for linear elastodynamics. For the fluid, 10 Navier–Stokes elements are used. The interpolation of the element geometry in time is linear or alternatively quadratic. An interface element between structure and fluid connects the subsystems. The spatial discretization is capable of describing the pressure and the velocity field exactly, since the pressure

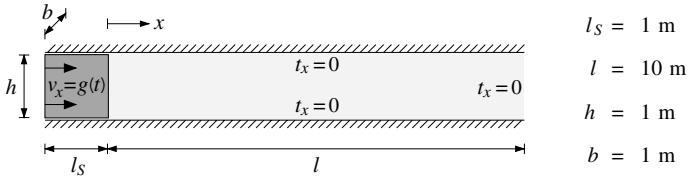

Fig. 3. System configuration of the piston example.

distribution is constant in the structure and linear in the fluid domain, while the velocity distribution is linear in the structure and constant in the fluid domain. In contrast, closed analytical solutions do not exist in time direction. The pressure field at different times is shown in Fig. 4. Time histories of velocity, displacement and traction at the interface are given in Fig. 5 (left). These results are calculated with a time slab width of $\Delta t = 0.01$ s using a quadratic interpolation of the geometry in time and without considering all stabilization terms.

In the right diagram of Fig. 5 the relative error $|(\bar{v} - v)/v|$ of the approximated velocity $\bar{v}$ at time $t = 8$ s is shown over the time slab width for the linear and the quadratic interpolation of the geometry as well as for the stabilized formulation. Instead of the exact value of the velocity v, the numerical solution for a very small time slab width of $\Delta t = 10^{-4}$ s is used. The third order accuracy of the time-discontinuous Galerkin formulation can be achieved for the coupled fluid–structure system, if the continuous interpolation of the geometry is quadratic in time. Thus, the coupling and simultaneous solution procedures do not have any negative influence on the time integration scheme. However, with the exception of applications whose

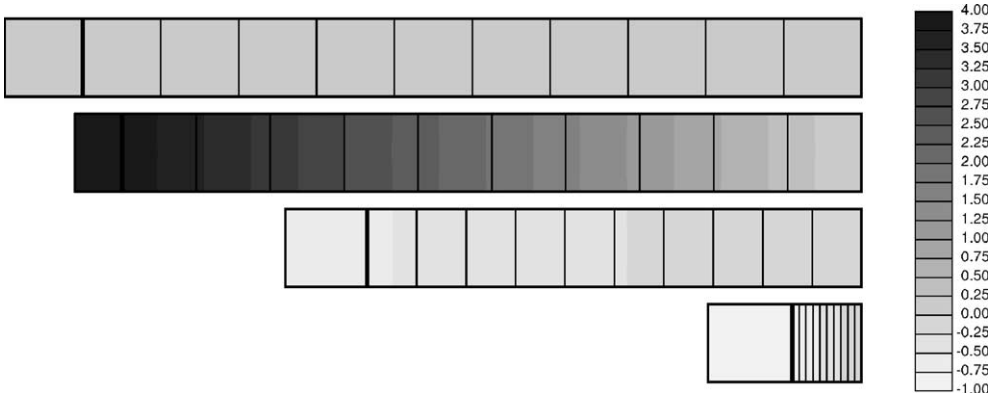

Fig. 4. Pressure fields at $t = 0.0$, 3.0, 6.0 and 9.5 s.

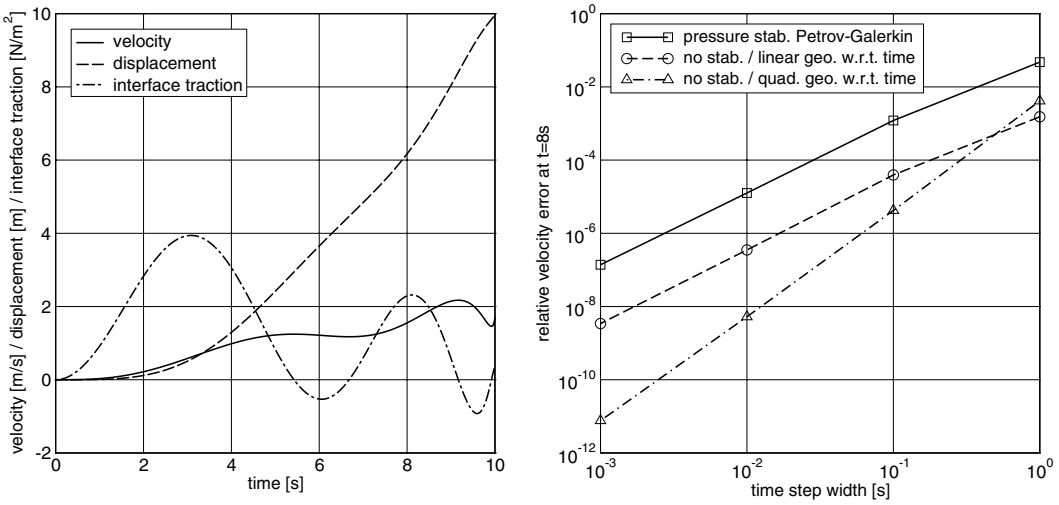

Fig. 5. Time histories and relative velocity errors.

spatial solution is exact, stabilized formulations are required in order to prevent spurious oscillations in the pressure field. In this case, only second order accuracy is achieved for the fluid solution, even if the interpolation of the geometry is quadratic in time.

5.2. Flow over a building with elastic membrane roof

This example deals with viscous fluid flow around a building, interacting with nonlinear vibrations of the membrane roof prestressed by gravity. The fluid density is $\rho = 1.25$ kg/m^3 and the viscosity $\mu = 0.1$ N s/m^2, which is much larger than the viscosity of air. However, the main issue of this work is the simultaneous solution procedure for fluid–structure interaction problems. Turbulence modeling, which is necessary for simulating realistic wind flow, is not taken into account at present. The inflow velocity profile is defined by $v_x(y) = 35$ m/s $(y/350\text{ m})^{0.22}$ leading to a velocity of $v_x(5\text{ m}) = 13.75$ m/s at roof level. Thus, the Reynolds number becomes $Re \approx 1700$ using the membrane length of $l = 10$ m as the length scale. The thickness of the membrane is $h = 0.01$ m, while density, Young's modulus and Poisson's ratio are given by $\rho_0 = 10^3$ kg/m^3, $E = 10^9$ N/m^2 and $v = 0$, respectively. The system configuration with all dimensions and boundary conditions is shown in Fig. 6.

The fluid domain is discretized with about 11,000 space–time hexahedron-elements, while 100 elements are used for the membrane structure. The complete spatial finite element mesh and a detailed plot close to the leading edge are shown in Fig. 7. The black bold line in the right figure represents the boundary of the fluid domain and the grey bold line the fluid–structure interface. The time slab width is chosen to be $\Delta t = 0.005$ s. This relatively small value is not necessary for stability and required accuracy, but leads to an efficient time domain analysis. In every time slab, the fully coupled nonlinear system is solved within two to three Picard iteration steps, and the BiCGStab solver converges after a few iterations, if the solution of the previous time step provides good preestimates for the iterative solution procedures. Thus, even for larger time steps, the overall CPU-time will not be reduced.

At first, the flow around the building with fixed membrane roof is simulated. For defining the membrane shape, the initially horizontal and non-prestressed membrane is loaded by the 0.32-fold value of dead load, which is reduced in order to account for the impact of the mean fluid pressure. With the preestimated membrane displacements, the fluid mesh is defined applying the mesh moving scheme of Section 3.4. The simulation starts with the given inflow velocity profile in the entire fluid domain. After a few time steps with spurious pressure peaks, a divergence free velocity field is reached. A separation zone develops at the leading edge of the building, whereas vortex shedding occurs at the trailing edge. The vortices stay some time behind the building and increase until the diameter exceeds the building height, see snap-shots of the pressure field close to the building in Fig. 8. Subsequently, the vortices move downstream with the mean

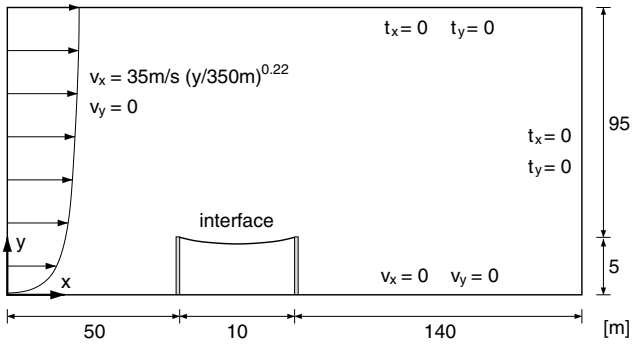

Fig. 6. System configuration for the flow over a membrane roof.

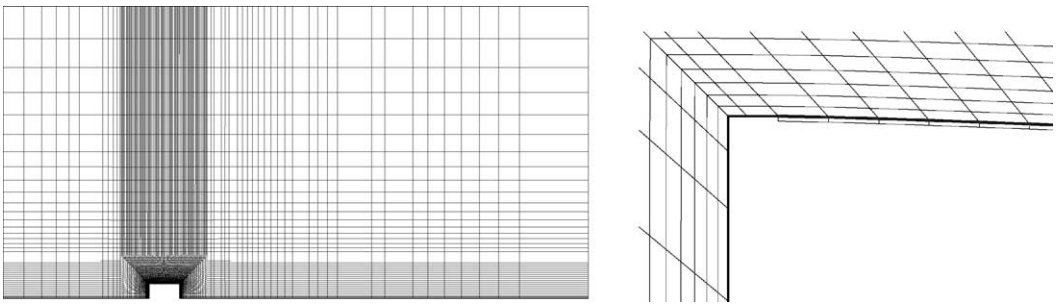

Fig. 7. Initial finite element mesh and detail close to the leading edge.

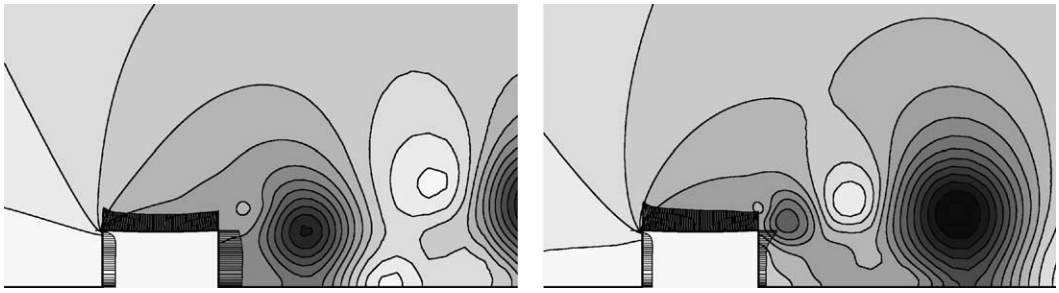

Fig. 8. Pressure fields at $t = 54.8$ and 57.8 s.

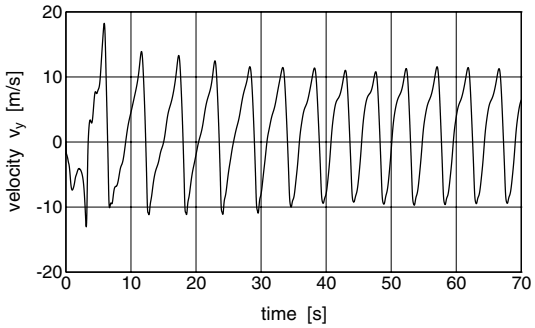

Fig. 9. Time history of the vertical fluid velocity behind the building.

flow, leading to a periodical system behavior with a frequency of $f = 0.21$ Hz. The time history of the vertical fluid velocity behind the building at $x = 67.5$ m and $y = 5.3$ m is shown in Fig. 9. After $t = 50$ s a periodic stationary behavior appears with relative small pressure variations at the membrane roof, since the flow field above the building is nearly vortex-free.

In order to obtain a smooth flow field above the building at the beginning of the coupled simulation, the solution for the fixed membrane at $t = 50$ s is used as initial condition. The first period of the coupled simulation is similar to the uncoupled flow behavior. Due to small pressure variations above the building, the membrane starts to oscillate, leading to the development of vortices directly behind the leading edge. The vortices move over the roof structure and induce membrane vibrations with large amplitudes, which

interact with the fluid. After some time, a more or less periodical system behavior occurs with a frequency of $f \approx 0.80$ Hz and displacement amplitudes in the membrane center of $u_y = 15$–20 cm. Due to strong nonlinearities in membrane kinematics and fluid dynamics, membrane vibrations and flow phenomena are not fully periodical. The time histories of vertical fluid velocity behind the building and membrane center displacement are shown in Fig. 10. The relatively high frequency of the coupled system is determined mainly by membrane dynamics, since the vortices, which are induced by membrane motions, pass the trailing edge without resting behind the building, see pressure fields in Fig. 11.

In this example, the flow around the building with elastic roof causes flow phenomena and effects on the membrane structure, which are quite different from the decoupled solution. Therefore, a strongly coupled simulation of membrane dynamics and viscous flow is preferable in order to predict accurately the behavior of the coupled system. Moreover, the monolithic approach leads to an efficient solution procedure, where the numerical effort for solving the coupled system is approximately the same as for the flow field only.

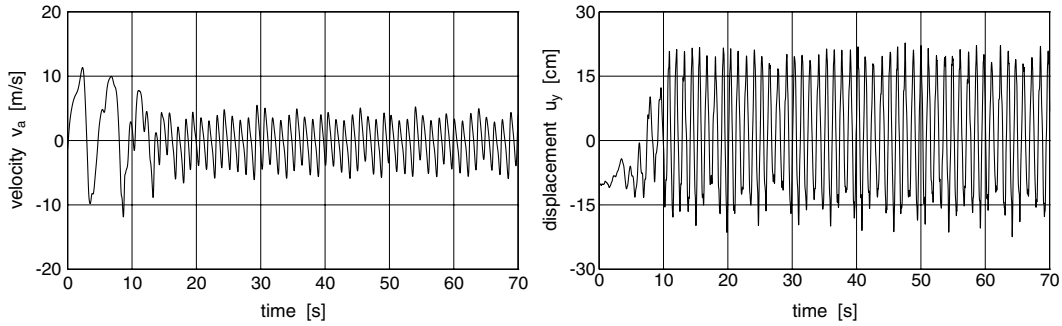

Fig. 10. Time histories of vertical fluid velocity and membrane center displacement.

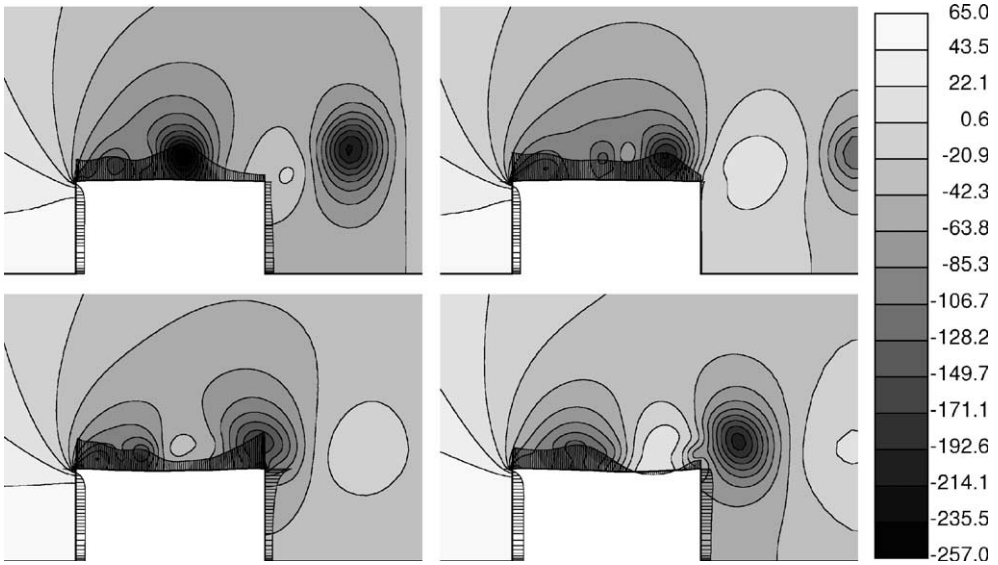

Fig. 11. Pressure fields in N/m^2 at $t = 67.0$, 67.4, 67.7 and 68.0 s.

5.3. Vortex excited elastic plate

A thin elastic cantilever plate is situated in the wake of a rigid square cylinder. Density, Young's modulus and Poisson's ratio of the plate structure are given by $\rho_0 = 2.0$ g/cm^3, $E = 2.0 \times 10^6$ g/(cm s^2) and $v = 0.35$, respectively. Density and viscosity of the fluid are given by $\rho = 1.18 \times 10^{-3}$ g/cm^3 and $\mu = 1.82 \times 10^{-4}$ g/(cm s), respectively. All dimensions and boundary conditions are shown in Fig. 12. Assuming an Euler–Bernoulli beam as a simplified model of the nonlinear plate structure, the first three natural frequencies become $f^S = 0.61$, 3.8 and 10.6 Hz. The example was proposed by Wall and Ramm [7]. However, a smaller inflow velocity of $v_x = 31.5$ cm/s is used here, leading to a Reynolds number of $Re = 204$, if the edge length of the square cylinder is used as the length scale. Fig. 13 shows the initial spatial finite element mesh with about 8 400 space–time elements for the fluid domain and 136 for the plate.

The system is investigated for both, a rigid and an elastic plate in order to compare the coupled system with the decoupled case. The time slab width is $\Delta t = 0.001$ s in each simulation. In the rigid case, vortex shedding occurs at the edges of the square cylinder, leading to a periodical system behavior with a frequency of $f^F = 3.7$ Hz. The vortices move over the fixed plate, and within each period two vortices appear on one side of the plate, while a larger one is situated on the other side, see Fig. 14. From this result, one may expect, the vortex configuration induces plate vibrations of small amplitude.

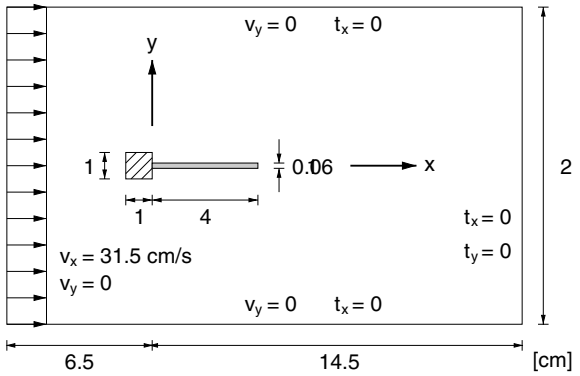

Fig. 12. System configuration for the vortex excited elastic plate.

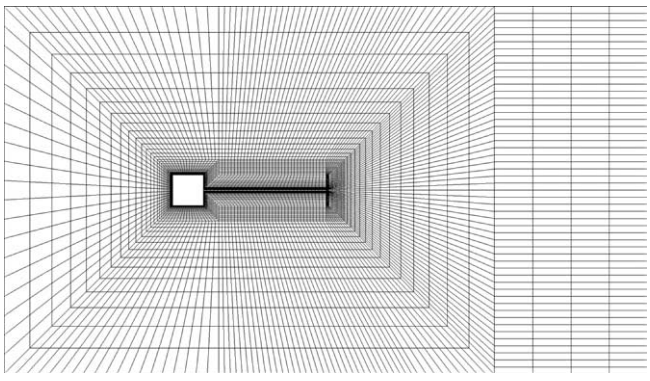

Fig. 13. Initial finite element mesh.

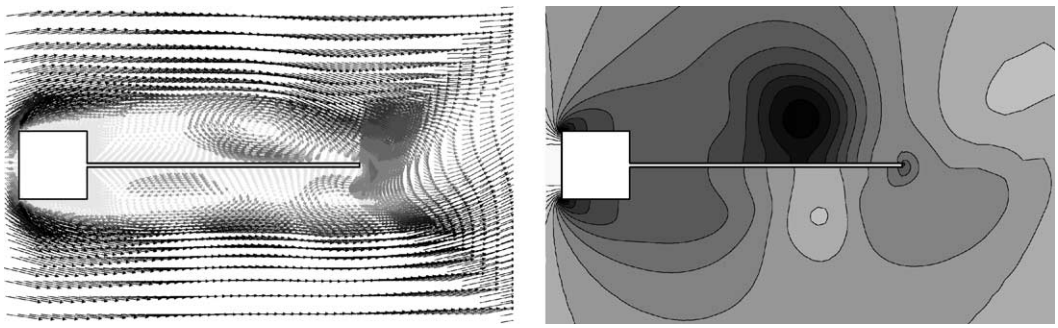

Fig. 14. Velocity and pressure field around the rigid plate.

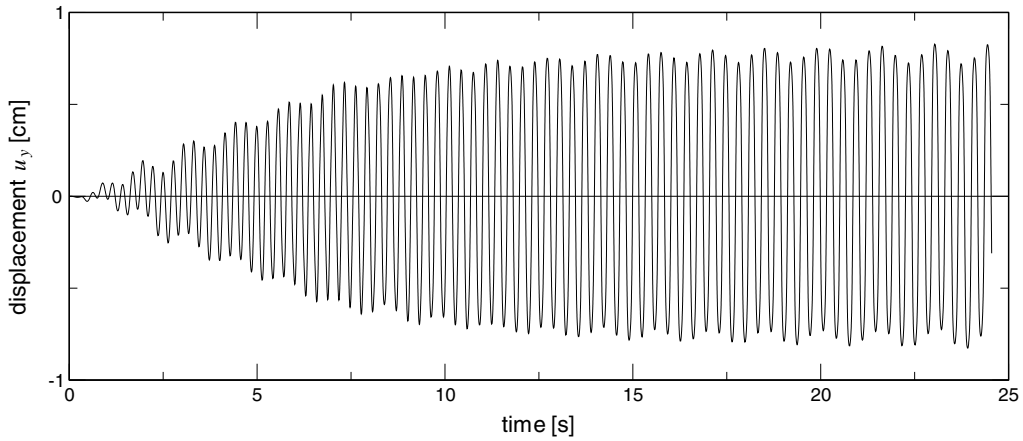

Fig. 15. Vertical tip displacement without initial deflection.

However, the coupled simulation leads to high amplitude plate vibrations with a maximum tip displacement of $u_y = 0.8$ cm, see the time history in Fig. 15. The frequency of the coupled motion of $f^{C} = 3.1$ Hz differs from the shedding frequency of the rigid plate of $f^{F} = 3.7$ Hz, although the second natural frequency of the plate of $f_2^{S} = 3.8$ Hz is close.

The coupled system behavior changes significantly, if the simulation starts with an initial deflection of $u_y \approx 2.3$ cm due to a temporary load, acting on the tip of the plate. Now, a periodic stationary solution is reached very quickly. The vibration frequency changes to $f^{C} = 0.8$ Hz, which is much lower than the frequency without initial deflection. The displacement amplitude increases more than twice and becomes $u_y = 2.0$ cm, see the left diagram in Fig. 16. In the right diagram, the resulting vertical fluid force, acting on the plate, is shown in addition to the tip displacement. A phase angle of $\varphi \approx \pi$ appears between fluid force and structural response, since the coupled vibration frequency is higher than the first natural frequency of the plate of $f_1^{S} = 0.61$ Hz, and structural damping is not considered. Pressure fields for half a period of the coupled motion are shown in Fig. 17. In contrast to the rigid case, a single large vortex dominates the flow field. At the tip of the plate, the vortex separates from the plate and induces a smaller vortex with opposite direction of rotation, leading to disturbances in the time history of the resulting fluid force.

In this example, the behavior of the coupled system differs clearly from the flow around the rigid structure. Strong interactions of fluid and structure govern the system response, and at least two stable

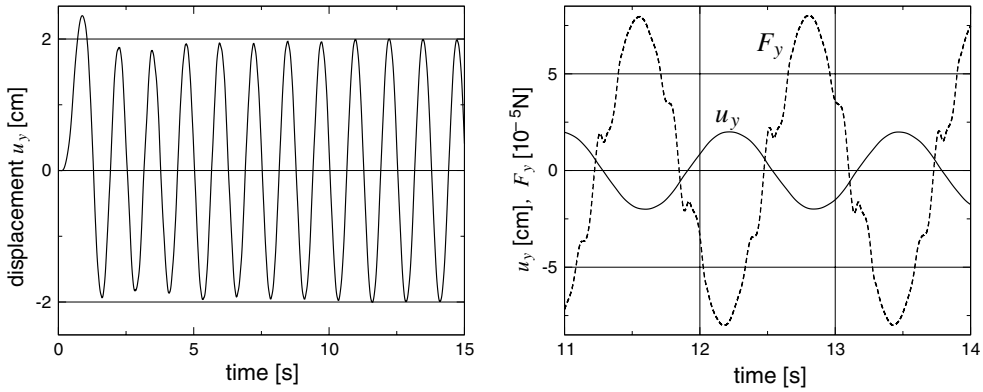

Fig. 16. Tip displacement and resulting vertical fluid force after initial deflection.

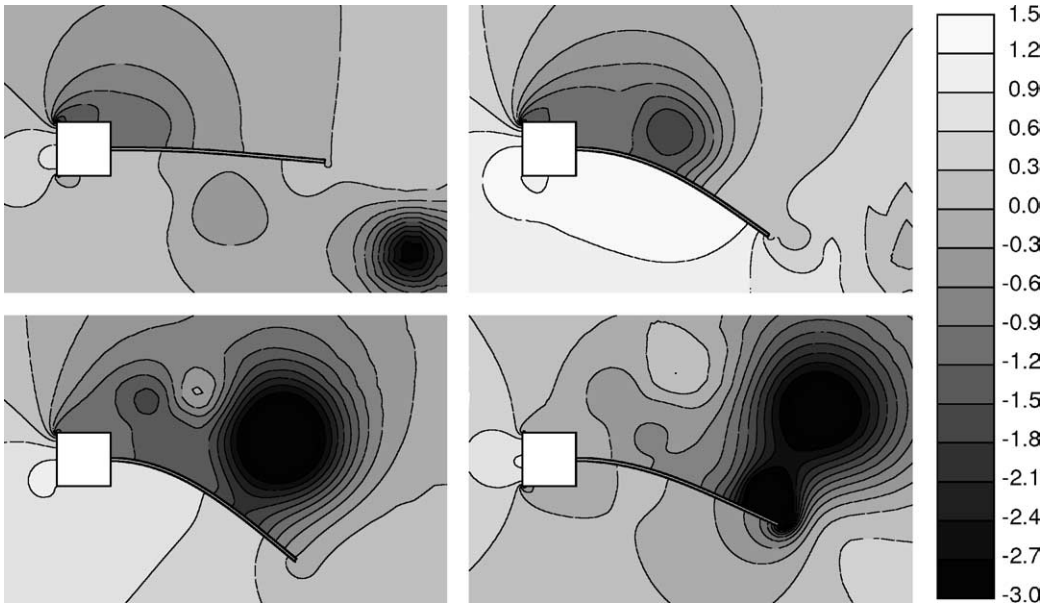

Fig. 17. Pressure fields in g/(cm s^2) at $t = 12.56$, 12.72, 12.92 and 13.04 s.

solutions exist. Thus, strongly coupled simulations are highly recommended in order to predict the right system characteristics for given initial configurations.

6. Concluding remarks

The paper presents a monolithic approach to the interaction of viscous fluid flow and geometrically nonlinear elastic structures, which is based on a uniform space–time finite element discretization. For the investigated two-dimensional numerical examples with strong interactions and large structural deformations, the procedure exhibits very good convergence properties with respect to the fully coupled nonlinear

solution. Thus, the monolithic approach seems to be an efficient solution procedure for coupled systems with strong interactions. However, a completely new implementation of the solver is required, which is conducted in an object-oriented program environment. In future, turbulence modeling, modeling of two phase flow and nonlinear material behavior will be included in the formulation.

Acknowledgements

This work was partially supported by the Deutsche Forschungsgemeinschaft (German Research Foundation) within the framework of the Graduiertenkolleg 432 ''Wechselwirkung von Struktur und Fluid''.

References

[1] E. Simiu, R.H. Scanlan, Wind Effects on Structures. Fundamentals and Applications to Design, John Wiley & Sons, New York, 1996.
[2] C.A. Taylor, T.J.R. Hughes, C.K. Zarins, Finite element modeling of blood flow in arteries, Comput. Methods Appl. Mech. Engrg. 158 (1998) 155–196.
[3] J.R. Cebral, R. Löhner, O. Soto, P.J. Yim, Finite element modeling of blood flow in healthy and diseased arteries, in: H.A. Mang, F.G. Rammerstorfer, J. Eberhardsteiner (Eds.), Proceedings of the Fifth World Congress on Computational Mechanics, Vienna, 2002.
[4] C.A. Felippa, K.-C. Park, Staggered transient analysis procedures for coupled-field mechanical systems: Formulation, Comput. Methods Appl. Mech. Engrg. 24 (1980) 61–111.
[5] R. Löhner, C. Yang, J. Cebral, J.D. Baum, H. Luo, D. Pelessone, C. Charman, Fluid–structure interaction using a loose coupling algorithm and adaptive unstructured grids, in: M. Hafez, K. Oshima (Eds.), Computational Fluid Dynamics Review 1995, John Wiley & Sons, Chichester, 1995.
[6] A. Masud, T.J.R. Hughes, A space–time Galerkin/least-squares finite element formulation of the Navier–Stokes equations for moving domain problems, Comput. Methods Appl. Mech. Engrg. 146 (1997) 91–126.
[7] W.A. Wall, E. Ramm, Fluid–structure interaction based upon a stabilized (ALE) finite element method, in: S. Idelsohn, E. Oñate, E. Dvorkin (Eds.), Computational Mechanics—New Trends and Applications (Proceedings of WCCM IV), CIMNE, Barcelona, 1998.
[8] C. Farhat, M. Lesoinne, Two efficient staggered algorithms for the serial and parallel solution of three-dimensional nonlinear transient aeroelastic problems, Comput. Methods Appl. Mech. Engrg. 182 (2000) 499–515.
[9] V. Kalro, T.E. Tezduyar, A parallel 3D computational method for fluid–structure interactions in parachute systems, Comput. Methods Appl. Mech. Engrg. 190 (2000) 321–332.
[10] P. Le Tallec, J. Mouro, Fluid structure interaction with large structural displacements, Comput. Methods Appl. Mech. Engrg. 190 (2001) 3039–3068.
[11] E. Ramm, W.A. Wall, Interaction of fluids and thin structures, in: Proceedings of the 2nd European Conference on Computational Mechanics, Cracow, 2001.
[12] S. Rugonyi, K.-J. Bathe, On finite element analysis of fluid flows fully coupled with structural interactions, Comput. Model. Engrg. Sci. 2 (2) (2001) 195–212.
[13] O.O. Bendiksen, A new approach to computational aeroelasticity, AIAA Paper 91-0939-CP, 1991.
[14] J.J. Alonso, A. Jameson, Fully-implicit time-marching aeroelastic solutions, AIAA Paper 94-0056, 1994.
[15] B.A. Grohmann, R. Dornberger, D. Dinkler, Time-discontinuous stabilized space–time finite elements for aeroelasticity, in: Fluid–Structure Interaction, Flow-Induced Vibrations and Noise, vol. 3 (AD53-3), ASME, 1997.
[16] F.J. Blom, A monolithical fluid–structure interaction algorithm applied to the piston problem, Comput. Methods Appl. Mech. Engrg. 167 (1998) 369–391.
[17] S.M. Rifai, Z. Johan, W.-P. Wang, J.-P. Grisval, T.J.R. Hughes, R.M. Ferencz, Multiphysics simulation of flow-induced vibrations and aeroelasticity on parallel computing platforms, Comput. Methods Appl. Mech. Engrg. 174 (1999) 393–417.
[18] B. Hübner, E. Walhorn, D. Dinkler, Strongly coupled analysis of fluid–structure interaction using space–time finite elements, in: Proceedings of the 2nd European Conference on Computational Mechanics, Cracow, 2001.
[19] M. Heil, J.P. White, Airway closure: surface-tension-driven non-axisymmetric instabilities of liquid-lined elastic rings, J. Fluid Mech. 462 (2002) 79–109.

[20] T.J.R. Hughes, G.M. Hulbert, Space–time finite element methods for elastodynamics: Formulations and error estimates, Comput. Methods Appl. Mech. Engrg. 66 (1988) 339–363.
[21] A.N. Brooks, T.J.R. Hughes, Streamline upwind/Petrov–Galerkin formulations for convection dominated flows with particular emphasis on the incompressible Navier–Stokes equations, Comput. Methods Appl. Mech. Engrg. 32 (1982) 199–259.
[22] T.J.R. Hughes, L.P. Franca, G.M. Hulbert, A new finite element formulation for computational fluid dynamics: VIII. The Galerkin/least-squares method for advective-diffusive equations, Comput. Methods Appl. Mech. Engrg. 73 (1989) 173–189.
[23] T.E. Tezduyar, M. Behr, J. Liou, A new strategy for finite element computations involving moving boundaries and interfaces—The deforming-spatial-domain/space–time procedure: I. The concept and the preliminary numerical tests, Comput. Methods Appl. Mech. Engrg. 94 (1992) 339–351.
[24] P. Hansbo, The characteristic streamline diffusion method for the time-dependent incompressible Navier–Stokes equations, Comput. Methods Appl. Mech. Engrg. 99 (1992) 171–186.
[25] M. Behr, T.E. Tezduyar, Finite element solution strategies for large-scale flow simulations, Comput. Methods Appl. Mech. Engrg. 112 (1994) 3–24.
[26] A.A. Johnson, T.E. Tezduyar, Mesh update strategies in parallel finite element computations of flow problems with moving boundaries and interfaces, Comput. Methods Appl. Mech. Engrg. 119 (1994) 73–94.
[27] D.C. Wilcox, Turbulence Modeling for CFD, DCW Industries, La Cañada, 1998.
[28] J. Knippers, R. Harbord, A mixed hybrid FE formulation for solution of elasto-viscoplastic problems. Part II: Dynamic loading conditions and bending problems, Comput. Mech. 13 (1994) 231–240.
[29] M. Lesoinne, C. Farhat, Geometric conservation laws for flow problems with moving boundaries and deformable meshes, and their impact on aeroelastic computations, Comput. Methods Appl. Mech. Engrg. 134 (1996) 71–90.
[30] G.M. Hulbert, Time finite element methods for structural dynamics, Int. J. Numer. Methods Engrg. 33 (1992) 307–331.
[31] C. Johnson, Discontinuous Galerkin finite element methods for second order hyperbolic problems, Comput. Methods Appl. Mech. Engrg. 107 (1993) 117–129.
[32] T.H.H. Pian, P. Tong, Basis of finite element methods for solid continua, Int. J. Numer. Methods Engrg. 1 (1969) 3–28.
[33] W.-M. Xue, L.A. Karlovitz, S.N. Atluri, On the existence and stability conditions for mixed-hybrid finite element solutions based on Reissner's variational principle, Int. J. Solids Struct. 21 (1) (1985) 97–116.
[34] J.C. Simo, R.L. Taylor, K.S. Pister, Variational and projection methods for the volume constraint in finite deformation elasto-plasticity, Comput. Methods Appl. Mech. Engrg. 51 (1985) 177–208.
[35] C. Farhat, M. Lesoinne, P. Le Tallec, Load and motion transfer algorithms for fluid/structure interaction problems with non-matching discrete interfaces: Momentum and energy conservation, optimal discretization and application to aeroelasticity, Comput. Methods Appl. Mech. Engrg. 157 (1998) 95–114.
[36] D.R. Lynch, Unified approach to simulation on deforming elements with application to phase change problems, J. Comput. Phys. 47 (1982) 387–411.
[37] J.H. Ferziger, M. Perić, Computational Methods for Fluid Dynamics, Springer, Berlin, 2002.